AIAA JOURNAL
Vol. 33, No. 3, March 1995

Effects of Chemistry on Blunt-Body Wake Structure

Virendra K. Dogra*
ViGYAN, Inc., Hampton, Virginia 23666
James N. Moss† and Richard G. Wilmoth*
NASA Langley Research Center, Hampton, Virginia 23681
and
Jeff C. Taylor‡ and H. A. Hassan§
North Carolina State University, Raleigh, North Carolina 27695

Results of a numerical study are presented for hypersonic low-density flow about a 70-deg blunt cone using direct simulation Monte Carlo (DSMC) and Navier–Stokes calculations. Particular emphasis is given to the effects of chemistry on the near-wake structure and on the surface quantities and the comparison of the DSMC results with the Navier–Stokes calculations. The flow conditions simulated are those experienced by a space vehicle at an altitude of 85 km and a velocity of 7 km/s during Earth entry. A steady vortex forms in the near wake for these freestream conditions for both chemically reactive and nonreactive air gas models. The size (axial length) of the vortex for the reactive air calculations is 25% larger than that of the nonreactive air calculations. The forebody surface quantities are less sensitive to the chemistry than the base surface quantities. The presence of the afterbody has no effect on the forebody flow structure or the surface quantities. The comparisons of DSMC and Navier–Stokes calculations show good agreement for the wake structure and the forebody surface quantities.

Nomenclature

A = base area of cone, $\pi d^2/4$
C_D = drag coefficient, $2D/\rho_\infty V_\infty^2 A$
C_f = skin-friction coefficient, $2\tau_w/\rho_\infty V_\infty^2$
C_H = heat transfer coefficient, $2q/\rho_\infty V_\infty^3$
C_p = pressure coefficient, $2p/\rho_\infty V_\infty^2$
D = drag
d = base diameter, 2 m
d_{ref} = molecular diameter at reference temperature
Kn = Knudsen number, λ/d
M = Mach number
$\mathcal{M}$ = molecular weight of air, 28.96 g/mole
$\mathcal{N}$ = Avogadro's number, 6.02252×10^{26} particles/kg-mole
N = atomic nitrogen
N_2 = molecular nitrogen
O = atomic oxygen
O_2 = molecular oxygen
p = pressure
q = heat flux
R_b = cone base radius
R_c = corner radius
Re = Reynolds number, $\rho V d/\mu$
Re_2 = total Reynolds number, $Re_\infty(\mu_\infty/\mu_{\text{stag}})$
R_n = cone nose radius
$\mathcal{R}$ = universal gas constant, 8.3143 J/mole-K
S = speed ratio, $V\sqrt{\mathcal{M}/2\mathcal{R}T}$
s = distance along the body surface measured from the stagnation point
$\bar{s}$ = temperature exponent of the coefficient of viscosity
T = thermodynamic temperature
T_{ov} = overall kinetic temperature
T_w = surface temperature
u = axial velocity
V = velocity
v = radial velocity
X = mole fraction
x = axial distance from stagnation point measured along symmetry axis
x_a = location of rear stagnation point
x_b = location of wake stagnation point
y = radial distance from symmetry axis
Γ = Gamma function
Δ = size of the vortex, $(x_b - x_a)/d$
λ = mean free path
μ = dynamic viscosity
ρ = density
σ = collision cross section
τ = shear stress

Subscripts

ref = reference value
stag = stagnation point
w = surface values
∞ = freestream values

Received Feb. 5, 1994; revision received Aug. 17, 1994; accepted for publication Aug. 20, 1994.

*Research Engineer. Associate Fellow AIAA.
†Research Engineer. Fellow AIAA.
‡Research Assistant, Department of Mechanical and Aerospace Engineering. Student Member AIAA.
§Professor, Department of Mechanical and Aerospace Engineering. Associate Fellow AIAA.

Introduction

THERE is a lack of experimental and computational data for blunt-body wake flows under rarefied flow conditions. Precise determination of wake closure is a critical issue for aerobrakes because the low lift-to-drag ratio aeroshell designs impose constraints on payload configuration. The payload must fit into the wake cone to minimize the heating since a heating spike is generally associated with reattachment of the separated flow in the near wake. Because of the complicated nature of the wake flow a perception exists[1] that the wake aerothermodynamics cannot be predicted accurately. A number of fundamental issues exist concerning such flows: 1) What role does thermochemical nonequilibrium play in the near wake? 2) How does the wake structure change as a function of rarefaction? 3) To what limits is the continuum modeling valid as rarefaction in the wake is progressively increased? Only recently, computational investigations[2–11] of blunt-body wake structure have begun to answer some of the previous questions and to

isolate critical features of the wake structure of planetary probes and aerobrakes.

Generally two methods are used to simulate the wake flows at high altitudes. One is the continuum approach in which a set of model equations is solved numerically, and normally this set is the Navier–Stokes equations. The Navier–Stokes modeling becomes inadequate for large local Knudsen numbers such as those occurring when the relatively high-density forebody flow expands into the wake. The second method is of a molecular nature where a direct physical simulation is done by following the motion and interaction of modeled molecules. This method is equally valid at low and high local Knudsen numbers, and therefore it is more appropriate to simulate the wake flows with the molecular method under rarefied conditions. In the present study, computational codes representative of both methods are used to simulate hypersonic wake flows about a 70-deg blunt cone. The molecular simulations are achieved with Bird's[12–14] direct simulation Monte Carlo (DSMC) method, whereas the continuum simulations are performed using the Navier–Stokes code developed by Olynick and Hassan[15] and Olynick et al.[16]

The purpose of the present paper is to provide an improved understanding of the effects of chemistry on blunt-body wake structure at flight conditions and to compare the results with Navier–Stokes calculations with slip boundary conditions. In addition, the DSMC calculations are also performed for a 70-deg blunt cone with a cylindrical as well as a proposed Mars Environmental Survey (MESUR) Pathfinder probe afterbody configurations.

Computational Method and Boundary Conditions

Both the molecular and continuum methods used in the present calculations are briefly described next.

Molecular Method

The direct simulation Monte Carlo (DSMC) method[12–14] is used for the present calculations. The method and requirements for application of DSMC have been presented in previous publications[17,18] and are not repeated here.

The computational domain used for the calculations is large enough to capture most of the body disturbance at the upstream and side boundaries. Thus, freestream conditions are specified at these boundaries. The flow at the downstream outflow boundary is supersonic, and vacuum conditions are specified.

The flowfield was divided into 18 regions and a fine grid resolution was used for cells in the wake regions. The cell dimension normal to the body surface in the forebody regions was on the order of half of the local mean free path. The cell dimension normal to the surface in the wake regions was less than the local mean free path. Further, study of grid resolution is given in Appendix A of Ref. 19. Steady state was assumed when the number of simulated molecules in each region achieved a fixed value within fluctuations of 1%. The average number of simulated molecules in a cell was 20 at steady state. The final results were obtained through a time-averaged solution over a large number of time steps.

The molecular collisions are simulated by the variable hard sphere (VHS) molecular model. This model employs the simple hard-sphere angular-scattering law so that all directions are equally possible for the postcollision velocity in the center-of-mass frame of reference. However, the collision cross section is a function of the relative energy in the collision. The freestream viscosity and mean free path are evaluated based on N_2 species using the VHS collision model with $T_{\text{ref}} = 2880$ K, $d_{\text{ref}} = 3.08 \times 10^{-10}$ m, and $\bar{s} = 0.73$. Energy exchange between the translational and internal modes is modeled by the Larsen–Borgnakke statistical model[20] with rotational and vibrational relaxation numbers of 5 and 50, respectively.

Continuum Method

The Navier–Stokes solver consists of an axisymmetric three-temperature, five-species implicit code. The set of equations solved consist of global mass, species mass, axial and radial momentum, global energy, rotational, and vibrational energy conservation equations. The code uses Roe's upwind scheme for the spatial inviscid fluxes, achieving second-order accuracy with the MUSCL scheme. The time integration is accomplished using an implicit lower-upper symmetric Gauss-Seidel (LU-SGS) scheme. This scheme was chosen because it only requires the inversion of a diagonal matrix at each point in the flowfield. With the large number of equations being solved, this is an attractive feature. A complete description of this method and modeling is presented in Ref. 15.

To account for the effects of the Knudsen layer that develops on the surfaces in low-density flows, slip boundary conditions are used. The modeling employed accounts for velocity, temperature, and species concentration slip effects. A more detailed description of the slip boundary conditions used is given in Ref. 16.

As shown in some previous comparisons between solutions using the DSMC method and the Navier–Stokes equations,[16] a meaningful comparison can be achieved provided the physical modelings employed by the two methods are matched as closely as possible. By doing this, the effects of using different physical models can be deduced, and the differences between the two solution procedures can be better observed. Thus, the chemical kinetic model and relaxation rates employed in the DSMC method[17] are also employed in the continuum calculations.

Freestream and Wall Conditions

The freestream conditions considered are those experienced by a typical space vehicle at an altitude of 85 km during Earth entry and are listed in Table 1. Three configurations—1) a 70-deg blunt cone, 2) a 70-deg blunt cone with cylindrical afterbody, and 3) a proposed Mars Environmental Survey (MESUR) Pathfinder probe body—are considered in the present calculations. The base diameter is 2.0 m for each of these configurations. Therefore, the forebody configuration is the same as that proposed[21] for the MESUR Network probes (16 total). Since the current MESUR Pathfinder probe has a 2.65-m base diameter, the third configuration is the scaled Pathfinder probe. These configurations are shown in Fig. 1. The freestream parameters along with selected results are summarized in Table 2. The freestream mean free path is based on the VHS model, and it is calculated from the relation (see Ref. 13)

$$\lambda_\infty = \frac{(T_\infty / T_{\text{ref}})^\omega}{\left[\sqrt{2} n_\infty \sigma_{\text{ref}} (2-\omega)^\omega \Gamma(2-\omega)\right]} \tag{1}$$

$$\omega = \bar{s} - \tfrac{1}{2} \tag{2}$$

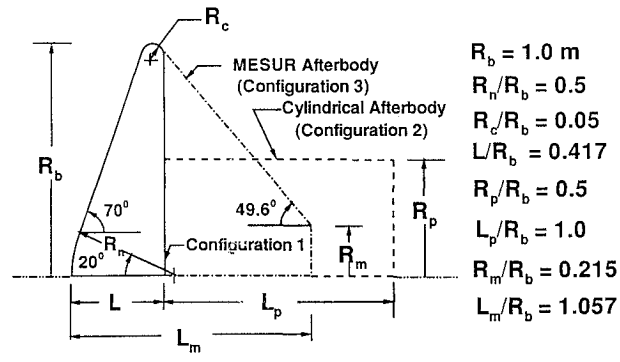

Fig. 1 Blunt cone and afterbody configurations.

Table 1 Freestream conditions[a]

Altitude, km	$\rho_\infty \times 10^6$, kg/m^3	V_∞, km/s	T_∞, K	M_∞	X_{O_2}	X_{N_2}	λ_∞, mm
85	7.955	7.0	180.65	25.98	0.2372	0.7628	7.189

[a] $T_w = 1000$ K and $\mathcal{M} = 28.96$ g/mole.

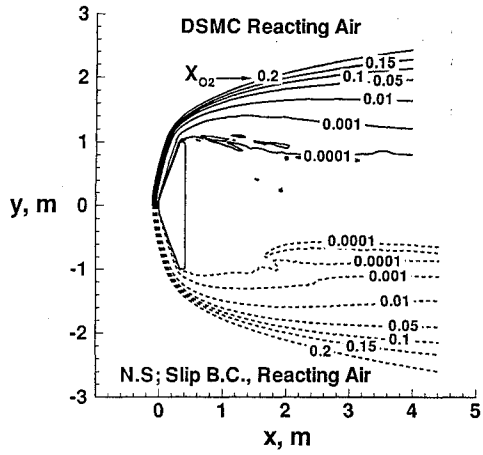

a) Molecular oxygen

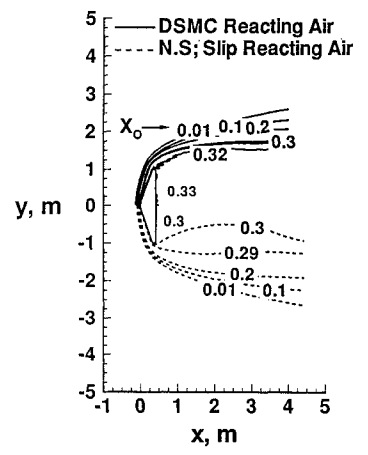

c) Atomic oxygen

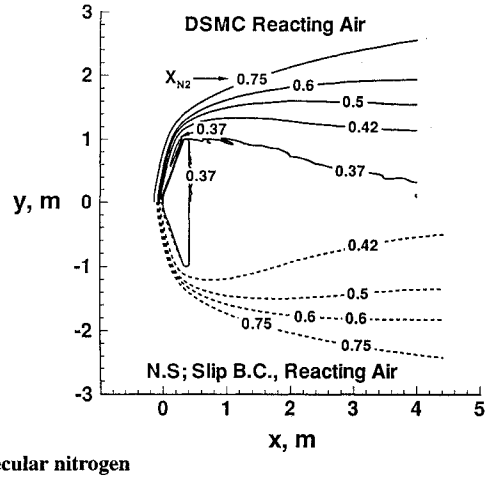

b) Molecular nitrogen

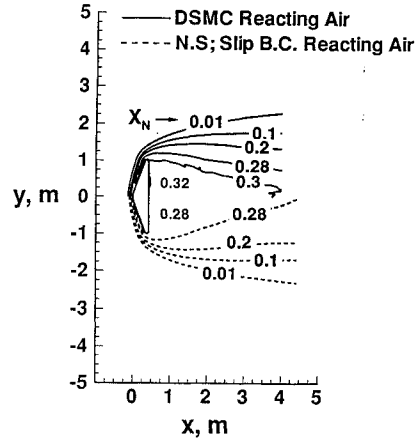

d) Atomic nitrogen

Fig. 2 Selected contours of species mole fraction (altitude = 85 km and Kn_∞ = 0.00359).

Table 2 Selected results and flow parameters[a]

Configuration	$C_{H_{stag}}$	$C_{P_{stag}}$	C_D	Δ
1	0.126	1.80	1.654	0.77
2	0.127	1.81	1.648	0.30
3	0.128	1.81	1.655	0.50

[a] Kn_∞ = 0.00359, S_∞ = 21.7, $Re_\infty = 9.033 \times 10^3$, and $Re_2 = 250.2 \times 10^{-2}$.

The gas-surface interaction is assumed to be diffuse with full thermal accommodation, and the surface temperature is assumed to be constant at 1000 K. The wall is also assumed as a noncatalytic surface. The chemical kinetics model[17] used is for 5 species (O_2, N_2, O, N, and NO) with 34 chemical reactions.

Results and Discussion

The DSMC and Navier–Stokes calculations were performed for a 70-deg blunt cone for the 85-km altitude during Earth entry conditions. Comparisons between the results are made with special attention given to the wake region as well as the surface results. In addition, DSMC calculations were also performed with cylindrical and Mars Environmental Survey (MESUR) Pathfinder probe afterbody configurations (scaled to 2.0-m base diameter). The grids selected for DSMC and Navier–Stokes calculations were such that the results are shown to be essentially grid independent (Ref. 19).

Chemistry Effects on Wake Structure

The dissociation of air is extensive for the current flow conditions as is clearly evident in Fig. 2. Figures 2a and 2b show that essentially all of the molecular oxygen and about half of the molecular nitrogen species are dissociated before reaching the body surface. The comparison of Figs. 2b–2d shows evidence of species separation among the heavy (N_2) and light (O and N) species as the flow expands into the wake region. Furthermore, the fluxes of O and N species are higher than the N_2 species flux to the base surface. Molecular nitrogen dominates the freestream, whereas the maximum concentration of atomic nitrogen occurs (Fig. 2d) just upstream of the corner expansion rather than along the stagnation streamline.

The sensitivity of the near-wake flow structure to chemical reactions can be seen in Figs. 3–5. The nondimensional density contours (Fig. 3a) and radial nondimensional density profiles (Fig. 4a) show that the densities in the near wake for the two gas models are not significantly different. The density in the near wake is less than 60% of the freestream value for both air models. The comparison of the overall kinetic temperature T_{ov} (defined as the weighted mean of the translational and the internal temperatures for a nonequilibrium gas) for reacting and nonreacting air is shown in Fig. 3b. It can be seen from this figure that the overall kinetic temperature in the near wake for the reacting gas is much lower than that of the nonreacting gas model because of the extensive amount of O_2 and N_2 dissociation occurring in the flowfield. The streamline plot shows that a steady vortex develops in the wake for both gas models (Fig. 3c).

Figure 4b presents the axial velocity profiles at three different axial locations in the wake. These profiles show that the shear-layer thickness changes very gradually along the downstream flow direction for both gas models. The axial velocity in the wake for the nonreacting gas is comparatively larger than the reacting gas model.

The wake stagnation point generally defined for separated symmetric flows is the location along the wake symmetry axis where the

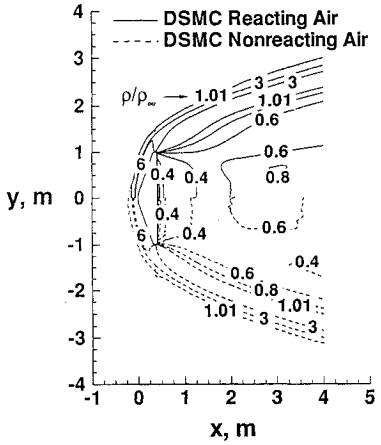

a) Nondimensional density, ρ/ρ_∞

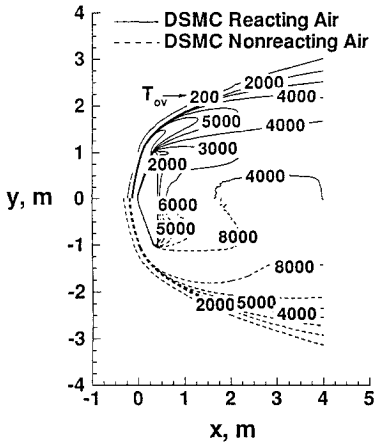

b) Overall kinetic temperature, T_{ov}

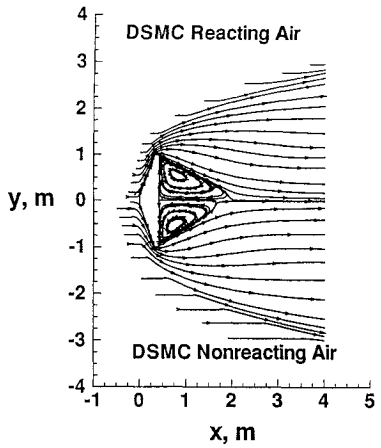

c) Streamlines

Fig. 3 Contours and streamlines (altitude = 85 km and Kn_∞ = 0.00359).

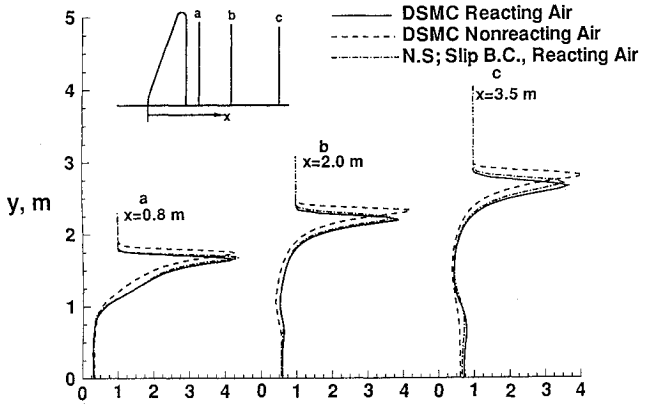

a) Nondimensional density, ρ/ρ_∞

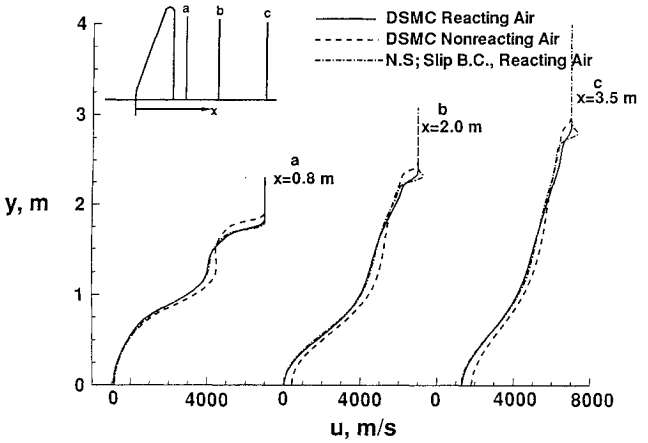

b) Axial velocity

Fig. 4 Wake profiles (altitude = 85 km and Kn_∞ = 0.00359).

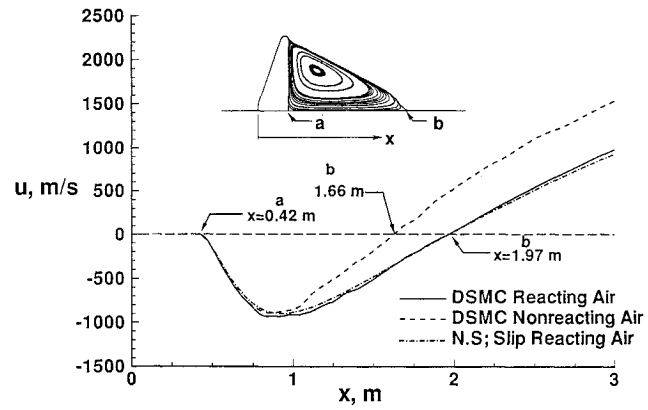

Fig. 5 Axial velocity along symmetry axis (altitude = 85 km and Kn_∞ = 0.00359).

flow velocity is zero. The effect of chemistry on the location of the wake stagnation point is shown in Fig. 5. The wake stagnation point for the reacting gas lies downstream of the wake stagnation point for the nonreacting gas. Therefore, the size (axial length) of the vortex Δ for the reacting gas is 25% larger than that of the nonreacting gas model.

Chemistry Effects on Surface Quantities

The effects of chemistry on surface pressure, heating rate, and skin friction are presented in Figs. 6a–6c, respectively. The results are shown as a function of the nondimensional distance (s/R_n) along the surface measured from the forebody stagnation point. The expansion of the flow at the corner reduces the base surface quantities many orders of magnitude compared with their forebody values. The effect of chemistry on surface pressure and skin friction is moderate, whereas the surface heating rate experiences a significant effect both in the forebody and the base regions. The stagnation point heating rate for the nonreacting gas is 49% higher than that of the reacting gas (Fig. 6b). The base heating rate for the nonreacting gas is more than 240% larger than the reacting gas model (Fig. 6b). But if the reacting gas calculations had been made with a finite or fully catalytic surface boundary condition, then this difference in surface heating would have been less. The minimum values of pressure and heating rate occur just before the flow expands onto the base surface (Figs. 6a and 6b). The chemistry model has essentially no effect on drag.

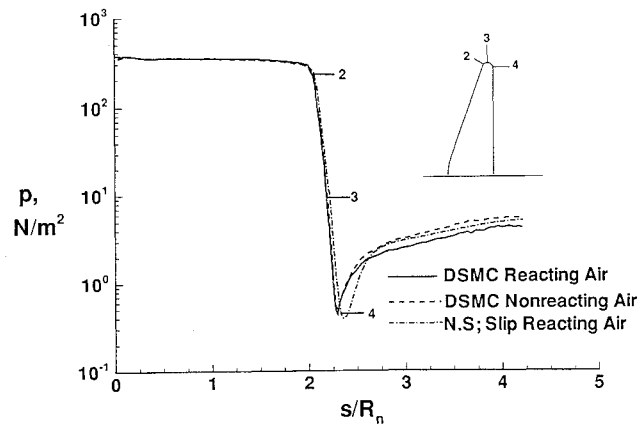

a) Surface pressure

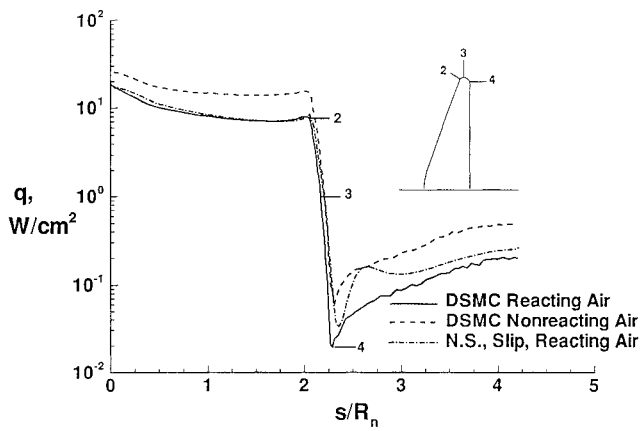

b) Surface heating rate

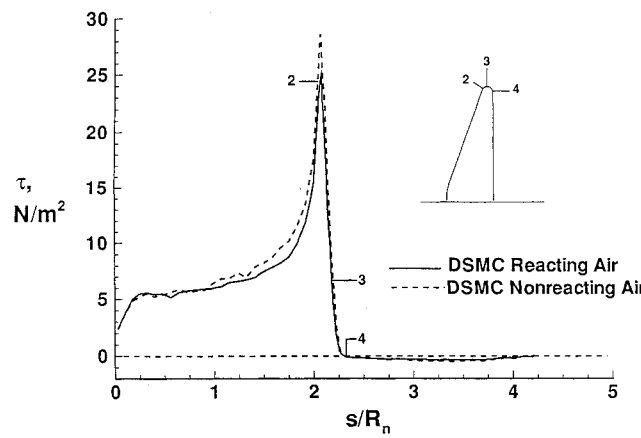

c) Skin friction

Fig. 6 Surface results (altitude = 85 km and Kn_∞ = 0.00359).

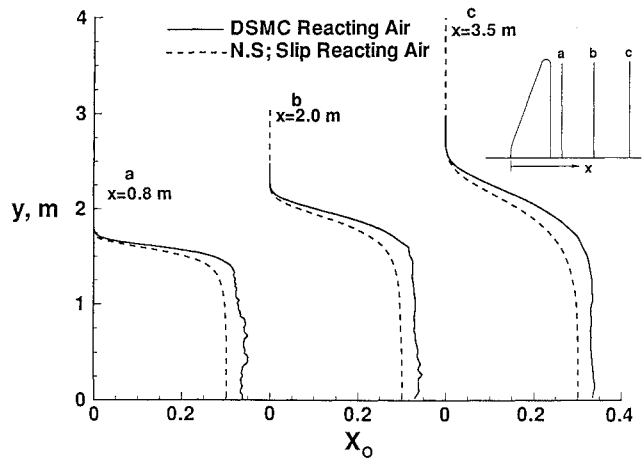

a) Atomic oxygen profiles

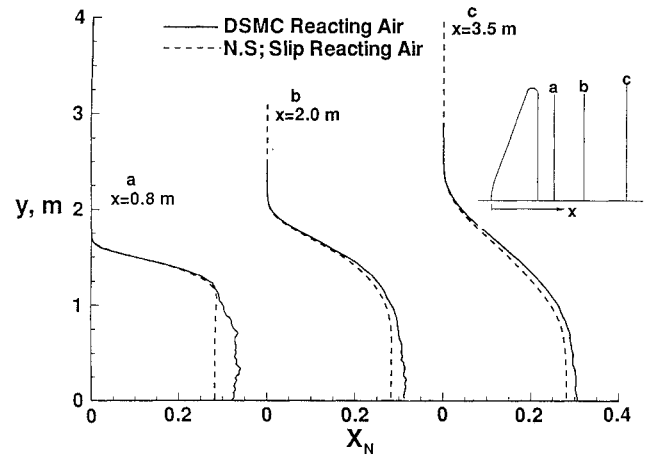

b) Atomic nitrogen profiles

Fig. 7 Mole fraction profiles (altitude = 85 km and Kn_∞ = 0.00359).

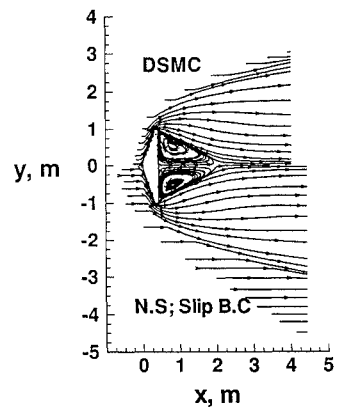

Fig. 8 Comparison of streamlines (altitude = 85 km and Kn_∞ = 0.00359).

Comparison of DSMC and Navier–Stokes Results

Comparisons of the chemical compositions from DSMC and Navier–Stokes calculations are shown in Fig. 2. Figures 2c and 2d show that the Navier–Stokes calculations predict slightly lower values of atomic oxygen and atomic nitrogen in the wake region compared with the DSMC results. The mole fraction of atomic oxygen in the wake region predicted by Navier–Stokes (with slip boundary condition) calculations is about 12% lower than that calculated by DSMC simulations (Fig. 7a), whereas the mole fraction of atomic nitrogen predicted by the Navier–Stokes calculations is about 18% lower near the base, and this difference decreases gradually in the downstream direction (Fig. 7b). The radial nondimensional density and axial velocity profiles (Figs. 4a and 4b) show very good agreement between DSMC and the Navier–Stokes calculations in the wake region. Figure 8 shows that both the DSMC and the Navier–Stokes calculations predict a steady vortex in the wake region, and furthermore both calculations predict the same size (axial length), $\Delta = 0.77$ (Fig. 5).

Comparisons of DSMC and Navier–Stokes (with slip boundary condition) calculations of the surface pressure and surface heating rate are shown in Figs. 6a and 6b. These surface quantities are shown in semilog scale as a function of nondimensional distance (s/R_n) along the surface measured from the stagnation point to give better perspective of the magnitudes along the base plane. Along the forebody, Navier–Stokes and DSMC results are in good agreement for both pressure and heating rate. The surface pressure and heating rate along the base surface calculated by Navier–Stokes calculations are generally higher than the DSMC results (Figs. 6a and 6b).

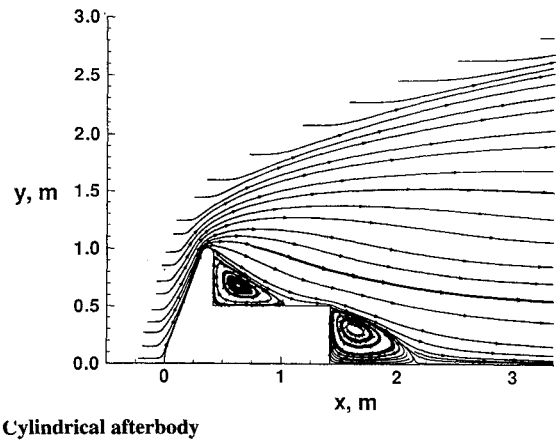

a) Cylindrical afterbody

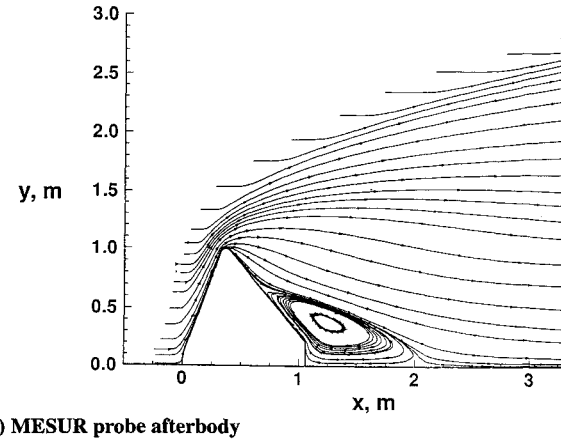

b) MESUR probe afterbody

Fig. 9 DSMC streamlines (altitude = 85 km and Kn_∞ = 0.00359).

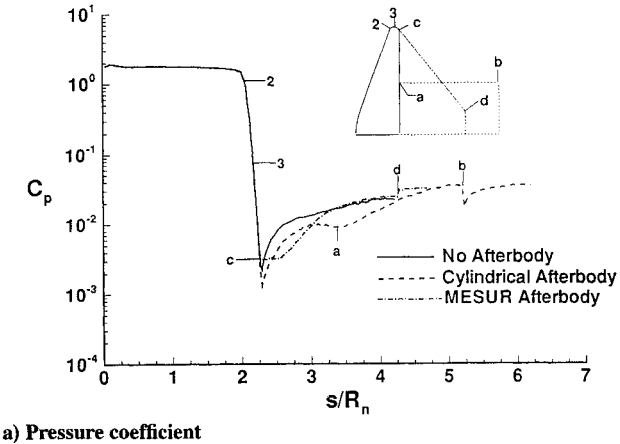

a) Pressure coefficient

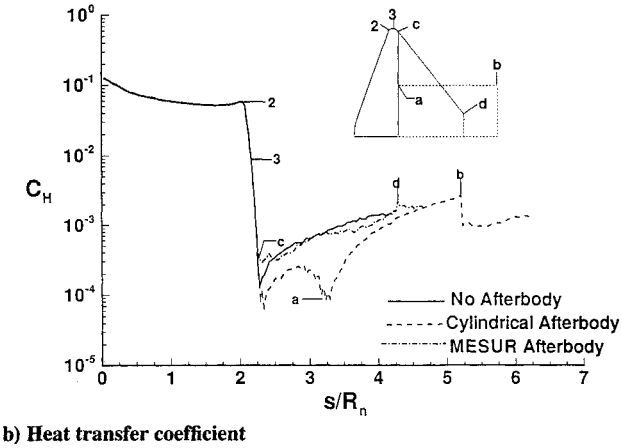

b) Heat transfer coefficient

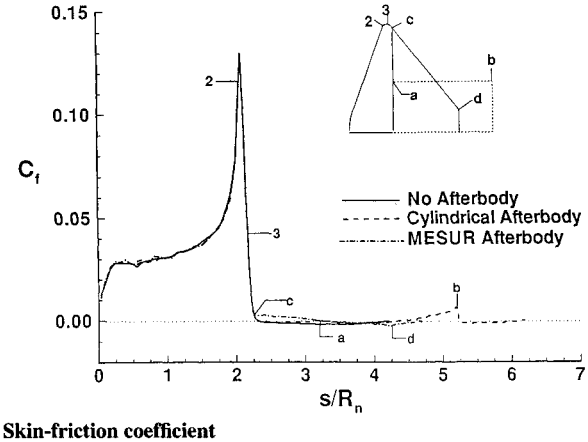

c) Skin-friction coefficient

Fig. 10 Effect of afterbody configurations on surface results (altitude = 85 km and Kn_∞ = 0.00359).

DSMC Calculations of the Blunt Body with Afterbody Configurations

DSMC calculations were also performed for a 70-deg blunt cone with two afterbody configurations: 1) a cylindrical afterbody and 2) a proposed afterbody configuration of the MESUR Pathfinder probe. These afterbody configurations were included to examine the impact on the surface heating and the flowfield features.

Figures 9a and 9b show streamline plots for the cylindrical and MESUR afterbody configurations, respectively. It can be seen from these figures that the cylindrical afterbody has developed two steady vortices (Fig. 9a), whereas for the MESUR afterbody only one steady vortex exists in the wake as shown in Fig. 9b. The comparisons of surface pressure, heat transfer, and skin-friction coefficients for the blunt body and two afterbody configurations are shown in Figs. 10a–10c, respectively. The distributions of surface pressure and heat transfer coefficients on the MESUR afterbody surface are very close to the distributions on the base surface of the blunt body (Figs. 10a and 10b), whereas for the cylindrical afterbody the heat transfer rate distribution on much of the afterbody surface is small compared with blunt-body base and MESUR afterbody surfaces.

Concluding Remarks

Axisymmetric DSMC and Navier–Stokes (with slip boundary conditions) calculations of flows about a 70-deg blunt cone have been performed for flow conditions experienced by a space vehicle at an altitude of 85 km and a velocity of 7 km/s during Earth entry. Particular emphasis is given to the effects of chemistry on the near-wake structure and the surface quantities. The surface quantities of the afterbody surface are also analyzed.

Essentially, all of the molecular oxygen and about half of the molecular nitrogen are dissociated before reaching the body surface. There is species separation among heavy (N_2) and light (O and N) species as the flow expands into the wake region. The density in the wake for the nonreacting gas model is slightly lower than the reacting model. The wake stagnation point for the reacting gas lies downstream of the nonreacting gas wake stagnation point. The base heating rate for the nonreacting gas is 240% larger than that of the reacting gas model with a noncatalytic surface. The comparison of the wake results predicted by the DSMC and the Navier–Stokes calculations shows good agreement for the flowfield quantities. The surface pressure and heating rate along the base surface calculated by the Navier–Stokes calculations are generally higher than the DSMC results. The presence of the afterbody has no effect on the forebody flowfield or the surface quantities.

Acknowledgment

Support for V. K. Dogra by NASA Contract NAS1-19237 is gratefully acknowledged.

References

[1]Anon., *America at the Threshold*, Report of the Synthesis Group on America's Space Exploration Initiative, Superintendent of Documents, U.S. Government Printing Office, Washington, DC, 1991, p. 59.

[2]Moss, J. N., and Price, J. M., "Direct Simulations of AFE Forebody and Wake Flow with Thermal Radiation," *Rarefied Gas Dynamics*, Vol. 118, edited by E. P. Muntz, D. P. Weaver, and D. H. Campbell, AIAA, Washington, DC, 1989, pp. 3413–3431.

[3]Gnoffo, P. A., Price, J. M., and Braun, R. D., "On the Computation of Near Wake, Aerobrake Flowfields," *Journal of Spacecraft and Rockets*, Vol. 29, No. 2, 1992, pp. 182–189.

[4]Dogra, V. K., Moss, J. N., Wilmoth, R. G., and Price, J. M., "Hypersonic Rarefied Flow Past Spheres Including Wake Structure," *Journal of Spacecraft and Rockets*, Vol. 31, No. 5, 1994, pp. 713–718.

[5]Brewer, E. B., "Hypersonic Rarefied Wake Characterization," NASA TP-3327, Jan. 1993.

[6]Lumpkin, F. E., Boyd, I. D., and Venkatapathy, E., "Comparison of Continuum and Particle Simulations of Expanding Rarefied Flows," AIAA Paper 93-0728, Jan. 1993.

[7]Dogra, V. K., Moss, J. N., Wilmoth, R. G., and Price, J. M., "DSMC Simulations of Hypersonic Low-Density Flow About an ASTV Including Wake Structure," *Rarefied Gas Dynamics: Space Science and Engineering*, edited by B. D. Shizgal and D. P. Weaver, Vol. 160, Progress in Astronautics and Aeronautics, AIAA, Washington, DC, 1994, pp. 199–208.

[8]Dogra, V. K., Moss, J. N., and Price, J. M., "Near-Wake Structure for a Generic Configuration of Aeroassisted Space Transfer Vehicles," *Journal of Spacecraft and Rockets*, Vol. 31, No. 6, 1994, pp. 953–959.

[9]Moss, J. N., Mitcheltree, R. A., Dogra, V. K., and Wilmoth, R. G., "Hypersonic Blunt Body Wake Computations Using DSMC and Navier-Stokes Solvers," AIAA Paper 93-2807, July 1993.

[10]Wilmoth, R. G., Mitcheltree, R. A., Moss, J. N., and Dogra, V. K., "Zonally-Decoupled DSMC Solutions of Hypersonic Blunt Body Wake Flows," AIAA Paper 93-2808, July 1993.

[11]Moss, J. N., Dogra, V. K., and Wilmoth, R. G., "DSMC Simulations of Mach 20 Nitrogen Flows About a 70-deg Blunted Cone and Its Wake," NASA TM 107762, Aug. 1993.

[12]Bird, G. A., *Molecular Gas Dynamics*, Clarendon Press, Oxford, England, UK, 1976.

[13]Bird, G. A., "Monte Carlo Simulation in Engineering Context," *Rarefied Gas Dynamics*, Vol. 74, Pt. I, edited by Sam S. Fisher, AIAA, New York, 1981, pp. 182–184.

[14]Bird, G. A., "Direct Simulation of Gas Flows at the Molecular Level," *Communications in Applied Numerical Method*, Vol. 4, No. 2, 1988, pp. 165–172.

[15]Olynick, D. R., and Hassan, H. A., "New Two-Temperature Dissociation Model for Reacting Flows," *Journal of Thermophysics and Heat Transfer*, Vol. 7, No. 4, 1993, pp. 687–696.

[16]Olynick, D. R., Taylor, J. C., and Hassan, H. A., "Comparisons Between DSMC and the Navier-Stokes Equations for Reentry Flows," AIAA Paper 93-2810, July 1993.

[17]Moss, J. N., and Bird, G. A., "Direct Simulations of Transitional Flow for Hypersonic Re-Entry Conditions," *Thermal Design of Aeroassisted Orbital Transfer Vehicles*, edited by H. F. Nelson, Vol. 96, Progress in Astronautics and Aeronautics, AIAA, New York, 1985, pp. 113–139.

[18]Dogra, V. K., Moss, J. N., and Simmonds, A. L., "Direct Simulations of Aerothermal Loads for an Aeroassist Flight Experiment Vehicle," AIAA Paper 87-1546, June 1987.

[19]Dogra, V. K., Moss, J. N., Wilmoth, R. G., Taylor, J. C., and Hassan, H. A., "Effects of Chemistry on Blunt Body Wake Structure," AIAA Paper 94-0352, Jan. 1994.

[20]Borgnakke, C., and Larsen, P. S., "Statistical Collision Model for Monte Carlo Simulation of Polyatomic Gas Mixture," *Journal of Computational Physics*, Vol. 18, No. 4, 1975, pp. 405–420.

[21]Tauber, M., Henline, W., Chargin, M., Papadopoulos, P., Chen, Y., Yang, L., and Hamm, K., "Mesur Probe Aerobrake Preliminary Design Study," AIAA Paper 92-2952, July 1992.